Parameter Variation of a Surface Acoustic Wave Motor

Philippus J. Feenstra, Peter C. Breedveld

Control Engineering Laboratory, Drebbel Institute for Mechatronics and Faculty of EEMCS,
University of Twente, P.O. Box 217, 7500 AE Enschede, Netherlands
{p.j.feenstra,p.c.breedveld}@utwente.nl

Abstract

This paper investigates the influence of parameter variation on the behavior of a Surface Acoustic Wave (SAW) motor. To this end, a model of the motor is used to vary the parameters independently. This model indicates that an increase of the friction coefficient, the Young modulus and the radius of the spheres at the bottom of the slider gives a raise in both the velocity and traction force.

1. Introduction

A Surface Acoustic Wave (SAW) motor is based on the elliptical motion of surface particles. A propagating SAW (Rayleigh wave) generates this motion in the surface of a stator. By pressing a slider with a sufficient preload against the stator, a linear slider motion is generated due to friction, i.e. an alternation of slip and stick. (Planar and rotational motion is possible as well, e.g. [1, 2]). The surface of the slider consists of spheres in order to eliminate air films and to optimize power transfer.

Like other Ultra Sonic Motors (USM), a SAW motor can generate a high force at low speed. Therefore, a compact construction with low noise is possible by circumventing a transmission box. Furthermore, the motion blocks in absence of waves, i.e. when no power is applied, no inherent magnetic fields are required due to the use of piezo electric material and no lubrication is needed.

In order to design a SAW motor with prescribed specifications (e.g. force-velocity relation) it is helpful to use design parameters, i.e. the required choice of material and geometry for a SAW motor in order to satisfy these specifications. To get a first impression of the design parameters, the influence of parameter variations on the motor behavior is investigated by means of a contact point model. Among the material parameters that can be varied are the friction coefficient and the Young modulus of stator and slider material. Besides material parameters, a geometric parameter, the radius of the contact spheres of the slider, is examined.

In the past, some work has been performed to obtain 'better' specifications. For example, Hélin [3] did an experiment with sliders with different friction coefficients, Nakamura et al [4] investigated the hardness (which is related to the shear modulus G) and Kurosawa et al [5] studied the influence of the contact point radius and the number of contact points. However, in practice there is always a dependency between parameters, whereas the use of a model has the advantage that parameters can be varied independently. Furthermore, not-measurable behavior can be examined and not practical parameters values can be investigated to find tendencies or for explanatorily reasons.

Section 2 describes briefly an experimental reference set-up. In section 3 the contact point model is described. Section 4 discusses the results. Some conclusions are given in section 5.

2. Analysis

This section briefly describes the experimental set-up, see figure 1. This set-up is used as basis for the contact point model, which is described in next section.

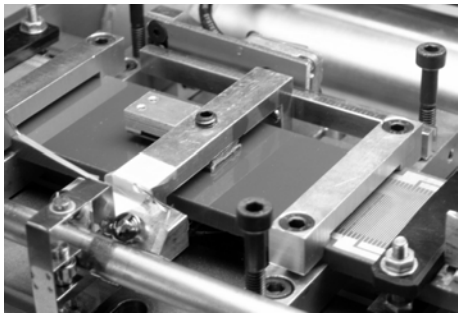

Figure 1: Experimental set-up

The stator ($160 \cdot 35 \cdot 5$ mm) made of PZT (Morgan Electro Ceramics, PXE 43) is used as waveguide. Interdigital transducers (IDT's) can generate SAW's at both ends of the stator. Each IDT has 20 finger pairs. The slider ($10 \cdot 10 \cdot 1$ mm) is made of silicon and has 40000 sphere shaped contact point, see figure 2. The slider motion is constrained by a guiding. Permanent magnets and an additional flux guiding generate a variable and measurable preload.

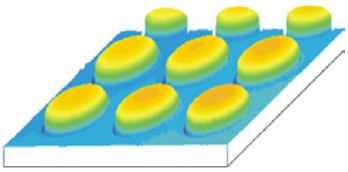

Figure 2: Spherical shaped contact points at the bottom of the slider.

3. Contact point model

In [6] a qualitative hybrid non-linear impact model is described. A simplified version of this model is used in this paper. This model describes the interaction between a SAW and one contact point of a slider. However, the qualitative behavior remains the same for multiple contact points because the SAW frequency lies far above the eigenfrequency of the contact mechanism. It can be shown that the coupling between the horizontal motion and the vertical motion is small. Therefore, it is admissible to model the horizontal motion separately, see figure 3(a). The inertia m is the total mass of slider and the guiding divided by the number of contact points. C_n is the normal non-linear stiffness between wave and slider for one contact point. v_n is the normal velocity of the elliptical motion and the open circle (a switched junction in bond graph terminology) detects whether there is contact between wave and slider. Furthermore, R_n represents the average squeeze-film air damping and F_p the gravitational force plus an additional applied preload force. The normal force P is used in the tangent model for the dry friction and the tangent stiffness.

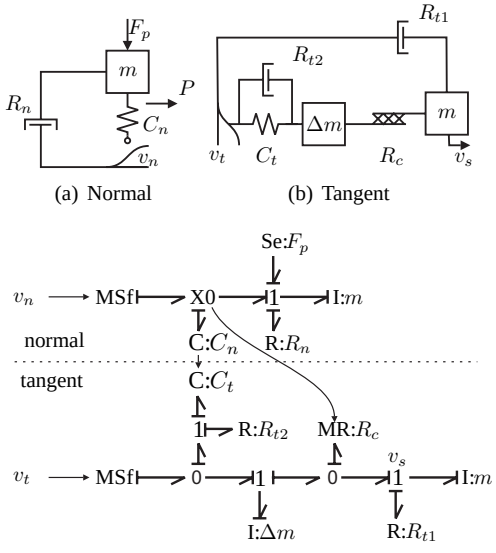

(a) Normal (b) Tangent

(c) Tangent and normal motion (bondgraph)

Figure 3: Model of contact mechanism

m	mass	1.565	mg
R	radius	1.37	mm
F_p	preload	0.25	mN
E_1	Young modulus Si	240	Gpa
E_2	Young modulus PZT	77	Gpa
σ_1	Poisson's ratio Si	0.3	-
σ_2	Poisson's ratio PZT	0.3	-
R_n	Normal damping	7	Ns/m
R_{t1}	Tangent damping	0.03	Ns/m
R_{t2}	Tangent damping	0.25	Ns/m
f	Frequency	2.2	MHz
μ	Friction coefficient	1	-

Table 1: Simulation parameters

Figure 3(b) shows the iconic diagram of the tangent motion. Again m represents the inertia and R_c models the dry friction by using a $\tanh$-function. The inertia Δm can be seen as the mass of the stator and slider that deforms, in other words: the mass-spring combination adds a mode of the deformation to the model. However, it has no dominant influence on the behavior, but it accounts for a preferred causality. C_t is a first order approximation of the tangent stiffness $F_c \approx 8aGz$, where F_c is the tangent force, z the tangent deformation, G the shear modulus and a the radius of the contact circle, which depends on the normal force P. The damping in tangent direction is modelled by R_{t1} and R_{t2}. v_t is the tangent velocity of the elliptical motion.

The model is implemented as bond-graph (figure 3(c)) in the simulation package 20-sim. The used integration method is *Vode Adams*.

4. Results

In this section the simulation results are described. The parameters that are varied are respectively the friction coefficient, the effective Young modulus and finally the radius of one contact point. The constant parameters are listed in table 1.

4.1. Friction coefficient

In this experiment, the kinetic friction coefficient is varied. In order to show the generic behavior, the range of the coefficient varies from a practical value of 0.1 to a rather unpractical value of 10. Figure 4 shows the static relation between steady-state velocity and friction coefficient for different wave amplitudes.

It demonstrates the existence of a certain optimal friction coefficient, which depends on the wave amplitude. The notion of stick and slip explains this phenomenon. First, note that the normal motion does not depend on the friction coefficient. Two limiting situations may be considered. Firstly, there is no (average) traction force if the friction coefficient is zero; accordingly, the slider velocity is zero. The contact continuously slips. Secondly, sup-

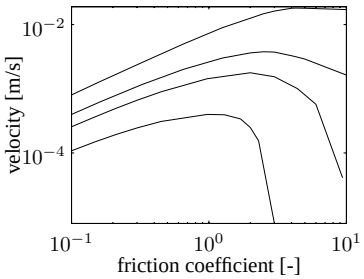

Figure 4: Steady state no-load velocity as a function of the friction coefficient. Wave amplitudes from top to bottom are $\{3, 1, 0.67, 0.3\}$ nm

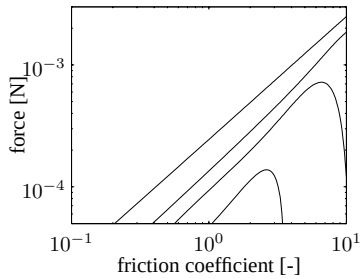

Figure 5: The average traction force as a function of the friction coefficient (slider velocity = 0). Wave amplitudes from top to bottom are $\{3, 1, 0.67, 0.3\}$ nm

pose that the friction coefficient is such that the contact continuously sticks. For example a friction coefficient of 4 if the wave amplitude is 0.3 nm, see figure 4. In this case, the average traction force is zero as well; hence, the slider velocity is zero. The optimum lies between those two limits. Moreover, the contact between slider and stator can be intermittent such that in this situation there cannot be a continuous stick. Then the velocity will not converge to zero, but there still remains an optimum. A similar explanation applies for the traction force, see figure 5. The optima shift due the difference in the time instants where stick and slip occur. The optima shift to the right because of larger relative velocity difference.

Furthermore, there is a close relationship with the so-called threshold amplitude. The threshold amplitude is defined as that wave amplitude at which the slider starts to move, e.g. if the friction coefficient is 2.4 then the slider moves in case the wave amplitude exceeds the threshold amplitude of 0.3 nm.

4.2. Normal and shear stiffness

In this experiment, the normal and shear contact stiffness are simultaneously varied. Assume that stator and slider are isotropic. Then the stiffness tensor depends on only two parameters; the Young modulus and Poisson's ratio. The normal and shear contact stiffness depend on both materials. Therefore, only one Young modulus is varied where the other, with a relative large value, is kept constant.

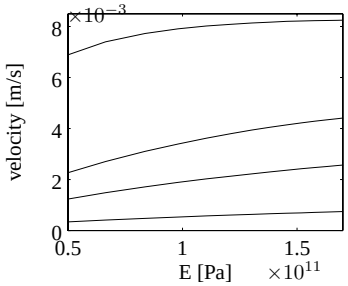

Figure 6: Steady state velocity as a function of the effective stiffness E. Wave amplitudes from top to bottom are $\{3, 1, 0.67, 0.3\}$ nm

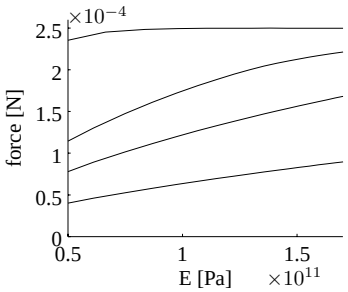

Figure 7: The average traction force as a function of the effective stiffness E. Wave amplitudes from top to bottom are $\{3, 1, 0.67, 0.3\}$ nm

Figure 6 shows the slider velocity as a function of the effective Young modulus, E,

$$E = \left(\frac{1-\sigma_1^2}{E_1} + \frac{1-\sigma_2^2}{E_2} \right)^{-1}$$

where E_1 and E_2 are the Young modulo and σ_1 and σ_2 the Poisson ratios of stator and slider. The figure demonstrates that the slider velocity increases if the normal (and shear stiffness) increases. For explanation, consider the normal motion. By increasing the normal stiffness, the maximal and minimal value of the normal force respectively increases and decreases, see figure 8. Hence, the traction force in positive direction becomes relatively larger than in the opposite direction, which explains the higher velocity. The influence of the shear stiffness on the velocity is marginal. The same explanation applies for the average traction force, figure 7. Here, one can see that the maximal force ($\mu F_p = 0.25N$) is reached at a wave amplitude of $3nm$.

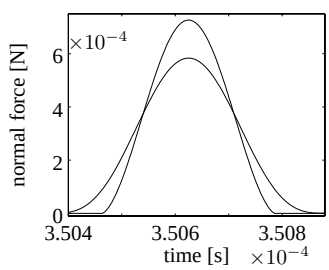

Figure 8: The normal force P as a function of time for two different effective Young modulus E. The normal force plot with the highest values has the largest E.

4.3. Radius of contact point

In this experiment the radius of a contact point is varied. Figure 9 shows that the slider velocity increases with the radius. The main reason of this tendency is again explained by the normal motion. An increase of the radius results in an increase in the normal (and shear) stiffness. Therefore, in accordance with section 4.2, the velocity will increase. Figure 10 shows the average traction force, which again reaches a maximum. It is important to note that the model is incompetent for large radii due to the assumption that the radius of the wave is larger than the radius of a contact point. Nevertheless it shows an increase in the slider velocity and traction force for larger radii.

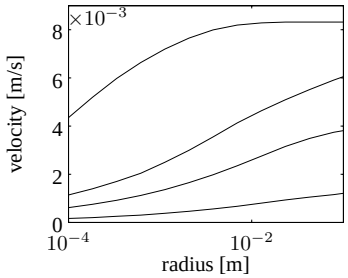

Figure 9: Steady state velocity as a function of the radius. Wave amplitudes from top to bottom are $\{3, 1, 0.67, 0.3\}$ nm

5. Discussion and conclusions

The influence of parameter variations on the motor behavior has been investigated by means of a contact point model.

Simulations show that there is a friction coefficient for which the velocity or the traction force is maximal. This optimal friction coefficient becomes un-physically large for large wave amplitudes. Therefore, one can conclude that a high friction coefficient is beneficial to obtain both high speed and high force at large wave amplitudes.

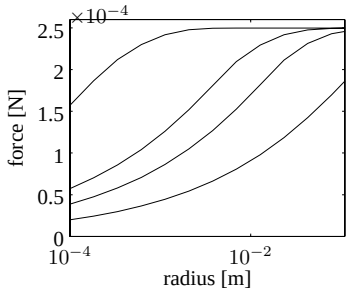

Figure 10: The average traction force as a function of the radius. Wave amplitudes from top to bottom are $\{3, 1, 0.67, 0.3\}$ nm

This conclusion is in accordance with Hélin's [3] experience. Furthermore, an increase of the contact stiffness increases both the velocity and the traction force. The contact stiffness can be increased by applying stiffer materials or by applying coatings. The contact stiffness can also be increased by increasing the radius of the contact spheres of the slider.

In future work this preliminary insight will be used to conduct experiments to validate the model. Moreover, the experiments are used to obtain design parameters.

6. References

[1] M. Vermeulen, F. Peeters, H. Soemers, P. Feenstra, and P. Breedveld, "Development of a surface acoustic wave planar motor under closed loop control," *3rd Euspen International Conference*, pp. 107–110, May 27-30 2002, eindhoven University of Technology, The Netherlands.

[2] L. Cheng, G. Zhang, S. Zhang, J. Yu, and X. Shui, "Minaturization of surface acoustic waves rotary motor," *Ultrasonics*, vol. 39, pp. 591–594, 2002.

[3] P. Hélin, "Theoretical and experimental studies of ultrasonic motors using lamb or rayleigh waves," Ph.D. dissertation, Univeristy of Valenciennes and Hainaut Cambrésis, December 12 1997.

[4] Y. Nakamura, M. K. Kurosawa, and T. Shigematusu, "Effects of ceramic thin film coating on friction surfaces for surface acoustic wave linear motor," in *IEEE International Ultrasonics Symposium, Honolulu*, 2003.

[5] M. Kurosawa, M. Takahashi, and T. Higuchi, "Optimum pre-load of surface acoustic wave motor," *IEEE International Ultrasonics Symposium, San Antonio, Texas*, November 1996.

[6] P. Feenstra and P. Breedveld, "Analysis of a surface acoustic wave motor," *IEEE International Ultrasonics Symposium, Honolulu*, 2003.